

Baroclinic adjustment and dissipative control of storm tracks

Article

Accepted Version

Novakova, L., Ambaum, M. H. P. ORCID:
<https://orcid.org/0000-0002-6824-8083> and Harvey, B. J.
ORCID: <https://orcid.org/0000-0002-6510-8181> (2018)
Baroclinic adjustment and dissipative control of storm tracks.
Journal of the Atmospheric Sciences, 75 (9). pp. 2955-2970.
ISSN 1520-0469 doi: <https://doi.org/10.1175/JAS-D-17-0210.1>
Available at <https://centaur.reading.ac.uk/77791/>

It is advisable to refer to the publisher's version if you intend to cite from the work. See [Guidance on citing](#).

To link to this article DOI: <http://dx.doi.org/10.1175/JAS-D-17-0210.1>

Publisher: American Meteorological Society

All outputs in CentAUR are protected by Intellectual Property Rights law, including copyright law. Copyright and IPR is retained by the creators or other copyright holders. Terms and conditions for use of this material are defined in the [End User Agreement](#).

www.reading.ac.uk/centaur

CentAUR

Central Archive at the University of Reading

Reading's research outputs online

1 **Baroclinic Adjustment and Dissipative Control of Storm Tracks**

2 LENKA NOVAK, * MAARTEN H. P. AMBAUM, AND BEN J. HARVEY

Department of Meteorology, University of Reading, Reading, United Kingdom

* *Corresponding author address:* Lenka Novak, Department of Meteorology, University of Reading, P.O. Box 243, Reading, RG6 6BB, United Kingdom.
E-mail: l.novakova@reading.ac.uk

ABSTRACT

3
4 The steady-state response of a mid-latitude storm track to large-scale extratropical thermal
5 forcing and eddy friction is investigated in a dry general circulation model with a zonally
6 symmetric forcing. A two-way equilibration is found between the relative responses of the
7 mean baroclinicity and baroclinic eddy intensity, whereby mean baroclinicity responds more
8 strongly to eddy friction whereas eddy intensity responds more strongly to the thermal
9 forcing of baroclinicity. These seemingly counter-intuitive responses are reconciled using
10 the steady state of a predator-prey relationship between baroclinicity and eddy intensity.
11 This relationship provides additional support for the well studied mechanism of baroclinic
12 adjustment in the Earth's atmosphere, as well as providing a new mechanism whereby eddy
13 dissipation controls the large-scale thermal structure of a baroclinically unstable atmosphere.
14 It is argued that these two mechanisms of baroclinic adjustment and dissipative control
15 should be used in tandem when considering storm track equilibration.

1. Introduction

Mid-latitude storm tracks are one of the primary drivers of regional and global climate variability, because they redistribute global heat, momentum and moisture. The long-term behavior of storm tracks is highly dependent on diabatic and frictional processes, but this dependency is complex and a major source of climate model biases (Harvey et al. 2013; Zappa et al. 2014, 2015; Pithan et al. 2016). The result is a large uncertainty in climate change predictions, reduction of which requires better understanding of the underlying dynamics (Shepherd 2014).

Storm tracks are characterized by maxima of baroclinic instability, arising from the radiative imbalance between the pole and equator. Within storm tracks available potential energy of the mean large-scale flow fuels eddies which in turn modify both the barotropic and baroclinic characteristics of the mean flow. The barotropic characteristics include jet latitude and wind speed, both of which are modified by eddy momentum fluxes. The baroclinic characteristics relate to the thermal properties of the mean flow, such as the mean meridional temperature gradient (which, by thermal wind balance, is proportional to the vertical shear of the mean flow). It is the interaction between the eddies and the baroclinic characteristics of the mean flow that is often seen as the primary control of mid-latitude storm tracks (e.g., Pedlosky 1992; James 1994; Novak et al. 2017).

Focusing therefore on this baroclinic eddy-mean flow interaction, Ambaum and Novak (2014) proposed a heuristic model that was later found to reproduce some detailed properties of the temporally oscillating behavior of the North Atlantic and North Pacific storm tracks (Novak et al. 2017). The model is a two-dimensional dynamical system:

$$\frac{ds}{dt} = F - f, \tag{1}$$

$$\frac{df}{dt} = 2f(s - D) \tag{2}$$

where $s = -kdT/dy$ is baroclinicity, and $f = kl^2[v^*T^*]$ is meridional eddy heat flux scaled by a constant, k , and a meridional wavenumber, l . Square brackets denote the zonal mean

41 and stars the perturbations thereof. Baroclinicity can be viewed as measuring the growth
42 rate of baroclinic eddies, and heat flux as measuring storm track activity (reflecting both
43 eddy density and intensity). The model assumes that the system is mainly forced by a
44 constant thermal forcing of the baroclinicity (F) and linearly damped by eddy dissipation
45 (Df). The assumption of a negligible eddy input and mean output can be justified using
46 observations of global energetics (Oort 1964), where most of the energy input is into the mean
47 available potential energy (proportional to global baroclinicity) and most of the output is
48 via frictional dissipation of eddy energy. The evolution of eddies (Eq. 2) is derived from
49 the unstable modes of baroclinic instability, where the generating rate by the background
50 baroclinicity is balanced by the dissipation rate of eddies. The reader is referred to Ambaum
51 and Novak (2014) for more a detailed discussion of this model.

52 The temporal evolution of Eq. 1 and 2 is analogous to an ecological predator-prey re-
53 lationship, whereby baroclinicity (prey) is periodically eroded by bursts of eddy heat flux
54 (predator) that mixes temperature horizontally downgradient. This relationship maintains
55 the system in a state that oscillates between being marginally stable and marginally unstable
56 with respect to the intense bursts in storm track activity (Novak et al. 2017). As Ambaum
57 and Novak (2014) noted, the value of baroclinicity around which the system oscillates be-
58 tween marginal stability and instability is equal to the eddy dissipation constant, D in Eq.
59 2.

60 In steady state, the Ambaum-Novak model predicts the following two-way equilibration.
61 Baroclinicity is independent of the thermal forcing that replenishes it in the time-varying
62 picture, but is proportional to eddy dissipation ($s = D$). On the other hand, steady-state
63 storm track activity is independent of the eddy dissipation that damps storm tracks in
64 the time-varying picture, but is proportional to thermal forcing of large-scale baroclinicity
65 ($f = F$).

66 Despite the idealized and perhaps counter-intuitive nature of the Ambaum-Novak model
67 predictions, existing numerical simulations of the ocean seem to agree with them. For ex-

68 ample in eddy-resolving models of the Southern Ocean, an increase in wind stress (forcing
69 of the mean baroclinicity) has been observed to be associated with insensitivity of the mean
70 baroclinicity but a rapid increase in eddy activity in steady state (Munday et al. 2013). This
71 process is called “eddy saturation”. Recent work of Marshall et al. (2017) has also shown that
72 changes in the bottom drag (via which eddy energy dissipates in the time-varying picture)
73 only affect the large-scale baroclinicity in steady state, whilst eddy energy remains largely
74 unaffected. Thus, Marshall et al. (2017) conclude that their results are consistent with the
75 Ambaum-Novak model predictions, except for the limiting cases of vanishing friction and
76 vanishing wind stress.

77 The atmospheric system is in some ways more complicated than the oceanic one, with the
78 location of eddy generation often coinciding with the location of eddy dissipation, especially
79 in more zonally uniform storm tracks, such as the one over the Southern Ocean. Moreover,
80 the radiative forcing of baroclinicity (as opposed to the wind-driven mechanical forcing in
81 the ocean) may directly result in large changes in static stability throughout the depth of
82 the atmosphere. Additionally, with the atmospheric storm tracks being closely interlinked
83 with the poleward edge of the Hadley cell, global changes in the radiative forcing or friction
84 can provide direct feedbacks from the tropics into the mid-latitudes and thus dominate the
85 steady-state responses (e.g. Mbengue and Schneider 2013; Polichtchouk and Shepherd 2016).

86 Furthermore, a lower thermal expansion coefficient in the oceans has been shown to be
87 associated with different eddy characteristics, such as larger scales of the eddies compared
88 to the deformation scale, reduced eddy diffusivity and the presence of barotropic inverse
89 cascades (Jansen and Ferrari 2012, Jansen and Ferrari 2013). The inverse cascade does
90 not dominate in the mid-latitude atmosphere (O’Gorman and Schneider 2007), due to the
91 Earth’s limited domain size relative to the deformation scale (Zurita-Gotor and Vallis 2009).
92 Baroclinic eddies therefore often interact directly with the mean barotropic flow, in addition
93 to being able to reduce the baroclinicity, and their barotropic feedbacks may substantially
94 intervene with the baroclinic eddy-mean flow interaction.

95 In spite of these additional complexities, the steady state of Eq. 1 (i.e. $f = F$) has
96 already been shown to hold approximately in the atmosphere. For example, vertical wind
97 shear has been observed to change only by 25 % compared to meridional eddy heat flux
98 variability of 280 % in response to seasonal changes in radiative thermal forcing (Stone
99 1978). Additionally, scaling arguments (Stone 1978; Jansen and Ferrari 2013) and GCM
100 modeling studies (Schneider and Walker 2006; Zurita-Gotor and Vallis 2009) have shown
101 that by being able to reduce the vertical wind shear and increase the static stability of the
102 mean flow, eddies can modify the isentropic slope (a measure of the mean baroclinicity)
103 to prevent it from becoming supercritical (steeper than unity), a process called baroclinic
104 adjustment (Stone 1978). It has also been found that under some parameter settings the
105 flow can in fact become supercritical, but sensitivity to thermal forcing is relatively low
106 compared to changing other parameters such as the planet size (Jansen and Ferrari 2013;
107 Zurita-Gotor and Vallis 2009). Additionally, for weak enough baroclinicity, static stability
108 change can dominate the eddy-induced baroclinic adjustment, leading to subcritical flows
109 (Schneider and Walker 2006). Nevertheless, the above studies agree that for parameters
110 close to Earth-like values, eddies maintain baroclinicity more or less insensitive to diabatic
111 forcing so that the isentropic slope remains close to unity.

112 The novel aspect of the steady-state prediction of the Ambaum-Novak model is that the
113 mean thermal wind is controlled by eddy dissipation (i.e. steady state of Eq. 2, $s = D$).
114 Eddy dissipation represents the combined effect of frictional and diabatic dissipation of eddies
115 as well as their advection out of the domain of interest. On Earth, it is the eddy friction
116 that dominates the total global eddy dissipation (e.g., Oort 1964).

117 Existing modeling experiments of the atmosphere suggest that the mean flow is sensitive
118 nonmonotonically to surface friction due to opposing effects of eddy and mean friction;
119 baroclinicity increases with increasing eddy friction when the total friction is strong but
120 also increases with increasing mean friction when the total friction is weak (Chen et al.
121 2007, Zurita-Gotor and Vallis 2009). In addition, Zhang et al. (2012) have found that for

122 sufficiently strong friction, increasing eddy friction increases the meridional temperature
123 gradient whilst leaving eddy kinetic energy largely unaffected in a quasi-geostrophic channel
124 model. These findings suggest that for strong enough friction the Ambaum-Novak argument
125 should work, but this conclusion is not robustly supported or tested in tandem with the
126 baroclinic adjustment mechanism by published studies.

127 Despite the promising findings above, there are some arguments that are seemingly con-
128 tradictory to the Ambaum-Novak predictions. For example, Chen et al. (2007) have found
129 strong dependency of storm track activity to eddy frictional dissipation in a dry GCM, while
130 the predictions above are for eddies and eddy friction to be independent. Furthermore,
131 O’Gorman (2010) and O’Gorman and Schneider (2008) find that in an idealized GCM and
132 in more complex climate models the steady-state mean available potential energy is directly
133 proportional to the thermal mean forcing of the meridional temperature gradient, yet the
134 Ambaum-Novak model prediction is for these to be independent in the steady state.

135 This paper tests the Ambaum-Novak model predictions in tandem, using a dry intermediate-
136 complexity GCM with a zonally uniform storm track. Using this GCM setup allows the
137 diabatic forcing and eddy friction to be imposed separately whilst retaining the main re-
138 alistic features of an Earth-like atmospheric circulation. This would not be possible with
139 complex climate models or observations. In addition, the experiments are implemented in a
140 perpetual equinox so that the GCM can equilibrate, and its time mean can be compared to
141 the steady-state predictions of the Ambaum-Novak model. Understanding the sensitivity of
142 baroclinic eddies and mean baroclinicity is of high relevance for understanding storm track
143 equilibration in changing climates, as well as their sensitivity to drag parameterizations in
144 complex models (e.g., Pithan et al. 2016).

145 Section 2 describes the model and the set up of the experiments. In order to test the
146 Ambaum-Novak predictions, section 3 presents responses of baroclinicity and eddy heat
147 fluxes to thermal forcing and eddy friction. Section 4 tests the robustness of these predic-
148 tions using the responses of the eddy and mean baroclinic energy terms. Section 5 further

149 investigates responses of the isentropic slope and criticality. Section 6 summarizes the find-
 150 ings and discusses them in light of the existing literature.

151 2. Model setup

152 The Portable University Model of the Atmosphere (PUMA, Fraedrich et al. 1998) is a dry
 153 dynamical core of a global circulation spectral model based on that of Hoskins and Simmons
 154 (1975). The setting of twenty equally spaced sigma levels and T42 horizontal resolution
 155 (corresponding to 2.815°) was used, since this resolution was found to be sufficient for the
 156 study of similar mid-latitude dynamics in a similar GCM by Chen et al. (2007). Additionally,
 157 PUMA with this resolution was found to produce realistic storm tracks (e.g. Fraedrich et al.
 158 2005), which exhibit the predator and prey-like oscillations in baroclinicity and heat flux that
 159 were observed in the North Atlantic and North Pacific (Novak et al. 2017). All experiments
 160 were run for 21 years of perpetual equinox. The first spin-up year was discarded from the
 161 time-mean averages, following Fraedrich et al. (2005).

162 The diabatic and frictional effects in the GCM are imposed as in Held and Suarez (1994).
 163 More specifically, diabatic processes are represented by Newtonian cooling with a timescale,
 164 τ_T , and friction is Rayleigh damping of divergence (Δ) and vorticity (ζ) with a timescale,
 165 τ_F . The model equations are therefore forced as follows:

$$\frac{\partial T}{\partial t} = \dots - \frac{T - T_r}{\tau_T} - H_T, \quad (3)$$

$$\frac{\partial \zeta, \Delta}{\partial t} = \dots - \frac{\zeta, \Delta}{\tau_F} - H_{\zeta, \Delta}, \quad (4)$$

167 where the H terms represent hyperdiffusion that parametrizes subgrid-scale mixing and
 168 dissipation. Both the thermal damping timescale, τ_T , and the frictional timescale, τ_F , are
 169 functions of height and τ_T is also a function of latitude.

170 In the control experiment τ_F is 1 day at the surface and increases to infinity at $\sigma = 0.7$. τ_T
 171 is 0.25 days at the equatorial surface and 40 days at the poles and in the upper troposphere.

172 There is no orography, and the pole to equator temperature difference of T_r is set to be 60 K,
173 and T_r is isothermal in the stratosphere. This setup is identical to that in Held and Suarez
174 (1994).

175 To test the Ambaum-Novak model predictions (i.e. $F = f$ and $s = D$), the equator-pole
176 heating/cooling profile of the GCM was varied in order to simulate changes in F , and eddy
177 friction was varied in order to simulate changes in D . Although diabatic thermal forcing and
178 eddy friction do not exclusively represent the total F and D (which also include advective
179 processes and eddy heating/cooling, both of which are difficult to impose locally externally),
180 they are nevertheless the dominant processes in zonally symmetric storm tracks such as those
181 considered here (e.g., Hoskins and Hodges 2005).

182 Explorative results (not presented) revealed that imposing eddy friction or thermal forc-
183 ing globally affects the stratification within the Hadley cell. This tropical response dominates
184 the response in the mid-latitude storm track intensity and latitude, agreeing with the exper-
185 iments of Polichtchouk and Shepherd (2016) and Mbengue and Schneider (2018). However,
186 since responses of the Hadley cell are not the focus of this study, both the thermal forcing
187 and eddy friction changes were limited to higher latitudes with their weighting functions
188 displayed in Fig. 1. Note that the general results are not sensitive to the precise form of
189 these weighting functions, as long as the strong tropical response is not triggered.

190 The thermal forcing was imposed by adding a barotropic tropospheric polar anomaly to
191 the time-invariant temperature field towards which the model is restored (i.e., T_r in Eq. 3).
192 Cooling over the polar region increases the large-scale meridional temperature gradient in the
193 T_r field, thus acting as a positive thermal forcing of the large-scale baroclinicity. Centering
194 the temperature anomaly over the poles ensures that the forcing of the baroclinicity is of the
195 same sign everywhere whilst still forcing the mid-latitudes substantially. Since the thermal
196 forcing and the restoration temperature field are zonally symmetric, only the zonal mean
197 baroclinicity is being forced directly. The “polar T anomaly” in the plots below refers to
198 the maximum value of this barotropic temperature anomaly, which is highest over the poles

199 and decreases towards the equator (as shown by the dashed line in Fig. 1).

200 Note that even though a large part of the heating/cooling is applied outside of the storm
201 track region, the large-scale temperature gradients that the baroclinic eddies feed on are
202 nevertheless affected substantially. The storm track therefore responds by equilibrating as
203 shown in the following sections. Repeating these experiments with a forcing that extends
204 further into the mid-latitudes (not shown) triggers the dominant tropical response discussed
205 above.

206 In our results below, the forcing is diagnosed as T_R/τ_T , rather than $(T_R - T)/\tau_T$, in
207 order to cleanly isolate the atmospheric adjustment to the external forcing from the external
208 forcing itself. However, the difference between the two ways of characterizing the forcing
209 is quite small since temperature damping term of the Newtonian cooling responds in such
210 a way that it increases slightly where T_R/τ_T is forced to increase and vice versa. It was
211 found that, for example, a 60K to 50K meridional temperature difference in the T_R gradient
212 corresponds to a 20% change in the “ T_R -only forcing” and 35% in the “ $T_R - T$ forcing”. The
213 result would be slightly more sensitive responses for the latter forcing but the conclusions
214 would remain the same.

215 Following Chen et al. (2007), changes in the frictional timescale (τ_F) were applied only
216 to zonal wavenumbers larger than zero, so as to limit these changes to eddies only. These
217 frictional changes were applied to a band of extratropical latitudes (weights shown by the
218 solid line in Fig. 1). Eddy dissipation can also be simulated in this idealized model setup
219 by changing the thermal relaxation timescale (τ_T). However, diabatic eddy processes act
220 as a sink of eddy energy in models with Newtonian cooling parameterizations, whereas in
221 the real world diabatic eddy processes are generally a source of eddy energy (e.g., Oort
222 1964). Nevertheless, for the sake of completion, a set of experiments where both the eddy
223 friction and eddy diabatic damping timescales were changed was conducted and yielded
224 qualitatively similar results (not shown). The small sensitivity of the response to the eddy
225 diabatic damping and the ambiguity over the role of eddy diabatic damping in the GCM are

226 the reasons why only the friction-based set of experiments is presented below. The “eddy
227 fric. timescale” in the plots below refers to the value of τ_F at the surface in the mid-latitudes
228 (where the solid line peaks in Fig. 1).

229 The results below are from a control run, 19 reference runs (where one of the thermal
230 forcing or eddy friction were being kept at the control value; these runs were used for spatial
231 analysis of the responses), and 70 runs where both thermal forcing and eddy friction were
232 changed (to indicate the robustness of the responses). The polar temperature anomaly range
233 is [-20, -17.5, -15, -12.5, -10, -7.5, -5, -2.5, 0, 2.5, 5, 7.5, 10, 12.5, 15] K and the frictional
234 time scale range is [0.5, 0.7, 1, 1.3, 1.6, 2] days. Although the thermal forcing and eddy
235 friction changes are imposed in different ways, their ranges were initially selected to have a
236 broadly similar mass-weighted effect. In other words, the friction only operates in the lowest
237 300 hPa and the maximum/minimum values of its range were selected to be a factor of 2
238 smaller/larger than in the control run. This is approximately equivalent to the factor of 1.3
239 for the same damping imposed over the whole tropospheric column (i.e. 800 hPa). This
240 factor was therefore applied to the thermal forcing. The choice of these ranges is justified
241 a posteriori by the similarity of the responses of the global circulation across these ranges
242 (shown in Section 2.b). Nevertheless, the precise choice of the ranges is not imperative for
243 the results presented below, as it does not affect the relative responses of heat flux and
244 baroclinicity.

245 *a. Control run*

246 The zonal and time averages of temperature, zonal wind, mean overturning circulation,
247 baroclinicity and eddy heat flux of the control run are displayed in Fig. 2. The heat flux,
248 $\overline{[v^*T^*]}$, is computed using the products of the meridional wind and temperature anomalies
249 from the zonal mean, where the square brackets denote zonal mean, stars are the departures
250 from it, and the bar is the time mean. Baroclinicity is diagnosed using the maximum Eady
251 growth rate (EGR), which is a common estimation of the linear growth rate of baroclinic

252 eddies (e.g., Hoskins and Valdes 1990):

$$\text{EGR} = 0.31f[\overline{N}]^{-1}[\overline{dU/dZ}], \quad (5)$$

253 where f is the Coriolis parameter, N the static stability, U the zonal wind, Z the geopotential height and the vertical gradient was calculated using the central difference method. The
254 mean overturning circulation is diagnosed using the mass streamfunction ($2\pi a \cos \phi g^{-1} \int_0^p [\overline{v}] dp'$).
255

256 Fig. 2 shows that the control run produces a clear subtropical jet, which has an extended
257 eddy-driven branch reaching lower levels on the poleward side, near the latitude of the maximum
258 of eddy heat flux and baroclinicity. The Hadley and Ferrel overturning cells are also
259 apparent. Since the control parameters were selected to mimic the Earth's atmosphere, comparison
260 with the ERA-40 Atlas (Kållberg et al. 2005) confirms that the wind and overturning
261 streamfunction patterns and values are comparable to the spring Southern Hemisphere with
262 both the subtropical and eddy-driven jets being present at 30° and 45° latitude, respectively.
263 The subtropical jet is a little weaker in PUMA and the Hadley cell is weaker in the upper
264 levels, which is expected in a system with no moisture (Kim and Lee 2001). The potential
265 temperature, eddy heat flux and baroclinicity fields are also comparable to the observed ones
266 (e.g. Kållberg et al. 2005; Novak et al. 2015).

267 *b. Location of circulation response*

268 To check that the response in the equatorward part of the Hadley cell does not dominate
269 the global response, Fig. 3 shows the vertically averaged overturning circulation and thermal
270 wind for the reference runs (i.e. where either eddy friction or thermal forcing is kept
271 constant). The Ferrel cell responds most strongly by shifting in latitude and only slightly
272 in strength. It moves poleward by about 5° with both reduced friction (i.e. increased eddy
273 friction timescales) and increased thermal forcing (i.e. a more negative polar temperature
274 anomaly). This shift is associated with the thermal wind developing a secondary maximum
275 on the poleward flank of the Hadley cell (associated with the subtropical jet) which maintains

276 the Hadley cell fixed equatorward of 30°N . Despite the similar latitudinal shifts in the Ferrel
277 cell for both thermal forcing and eddy friction, the strength of the associated thermal wind
278 maximum that marks the eddy-driven jet is much more sensitive to eddy friction than to the
279 thermal forcing. Because the thermal wind is closely related to baroclinicity, this response is
280 discussed further in the next section.

281 **3. Local baroclinicity and eddy heat flux**

282 Since the Ambaum-Novak predictions are based on the meridional eddy heat flux and
283 baroclinicity, Fig. 4a-d show these two quantities for the reference runs. Baroclinicity and
284 heat flux are computed as in the previous section, but here limited to 775 hPa and 850 hPa,
285 respectively (following Hoskins and Valdes 1990).

286 Although there is never complete insensitivity to either eddy friction or thermal forcing,
287 it is apparent that heat flux is more sensitive to the thermal forcing whereas baroclinicity
288 is more sensitive to the eddy friction. These responses concur with the Ambaum-Novak
289 prediction.

290 In accordance with the thermal wind in Fig. 3, Fig. 4e and f show that the meridional
291 temperature gradient responses almost mirror the spatial responses in baroclinicity. Con-
292 versely, static stability (Fig. 4g and h) mirrors the spatial response of the eddies which is
293 consistent with Schneider and Walker (2006)'s observation that eddies stabilize the large-
294 scale flow. For the strongest polar cooling, baroclinicity decreases slightly in intensity even
295 though the vertical wind shear is forced to increase. This is because the response in static
296 stability (N in Eq. 5) overcompensates slightly for the changes in the vertical wind shear in
297 these cases. This overcompensation has also been observed in GCMs used by Schneider and
298 Walker (2006) and Zurita-Gotor and Vallis (2009).

299 The rest of this section summarizes results of all forced experiments, where both the
300 eddy friction and thermal forcing were varied. Both low-level zonal-mean baroclinicity and

301 eddy heat flux were averaged over a baroclinic mixing zone, in order to isolate the region
302 where eddies are strong enough to drive the baroclinic equilibration (note that this was
303 not necessary in Marshall et al.'s (2017) channel model, where eddy equilibration occurred
304 throughout the whole domain). This mixing zone is defined as the latitudes where the low-
305 level eddy heat flux is at least 70% of its maximum value, following Schneider and Walker
306 (2008). As opposed to the latter study, the baroclinic zone in the current experiments
307 varies substantially in its meridional extent. This yields results that are not robust for
308 different thresholds of the heat flux percentage. To correct for this, the present study uses
309 the meridional width of the baroclinic zone of the control run (defined as above), centered
310 around the maxima in the heat flux of the forced runs. This method yields more robust
311 results for a wide range of heat flux thresholds used to define the mixing zone.

312 The results in Fig. 5 show that the two-way equilibration predicted by the Ambaum-
313 Novak model is evident. Baroclinicity and heat flux are proportional to the eddy friction
314 and thermal forcing respectively, with no strong relationships vice versa. These results
315 are qualitatively similar for any reasonable heat flux percentage values used to define the
316 baroclinic zone (e.g., zones defined using values of 30 - 80% of heat flux maximum).

317 A closer inspection of the responses reveals that they are relatively small compared to
318 the amount of thermal forcing or eddy friction applied. More specifically, for a factor of two
319 change in the equator-pole temperature gradient in the T_r field (i.e., the thermal forcing),
320 the heat flux increases by about 15%. On the other hand, a factor of four increase in eddy
321 friction leads to a 10% increase in baroclinicity. However, a one-to-one relationship between
322 the forcing/friction and the responses is not expected because of the inability to vary local
323 advective processes externally (as discussed in the previous section) and, more importantly,
324 because of the geographical restriction of the forcing/friction changes.

325 It is noted that stronger relationships between eddy friction and baroclinicity, and di-
326 abatic forcing and eddy fluxes have been observed independently in channel models used
327 by previous studies where such restrictions were not necessary (Zhang et al. 2012; Marshall

328 et al. 2017). However, it is the relative response of baroclinicity and heat flux (in a more
329 realistic atmosphere of a spherical GCM) that is of interest in the present study, rather than
330 the magnitude of the responses relative to the forcing/dissipation.

331 **4. Mean available potential energy and eddy energy**

332 The mean available potential energy (mean APE) can be viewed as the energy of the mean
333 thermal state that can be converted into eddies, and its variability in the mid-latitudes is
334 primarily modulated by eddy activity (Novak and Tailleux 2018). In fact, in an idealized
335 atmosphere with a constant horizontal temperature gradient, the quasi-geostrophic (QG)
336 form of APE (originally defined by Lorenz 1955) is proportional to the square of the domain-
337 integrated maximum Eady growth rate (Schneider 1981). Moreover, eddy energy (sum of
338 kinetic and available potential eddy energies) is a measure of eddy intensity. When diagnosed
339 locally within the storm track, the mean APE and eddy energy may therefore be regarded
340 as alternative measures of baroclinicity and storm track activity respectively. This section
341 uses these measures and further tests the Ambaum-Novak model predictions.

342 Many studies use Lorenz’s (1955) QG approximation to diagnose APE over the storm
343 track zone (e.g., O’Gorman and Schneider 2008; O’Gorman 2010). However, such local
344 calculations are in fact approximate estimates because a) they require the QG approximation
345 and b) Lorenz’s (1955) APE must be calculated over a domain with impermeable boundaries,
346 i.e. the global domain, in order to be formally correct.

347 Instead of using Lorenz’s (1955) classical definition of global APE, this analysis therefore
348 uses a version that does not require the QG approximation and can be formally defined
349 locally. Nevertheless, having repeated the analysis below for Lorenz’s (1955) QG APE
350 integrated over the baroclinic zone, it was found that both definitions yield qualitatively
351 similar results.

352 The local APE was first introduced by Holliday and McIntyre (1981) and Andrews (1981)

353 and recently adapted for diagnostic analysis in the atmosphere (Novak and Tailleux 2018).
 354 This local APE is essentially the vertical integral of the buoyancy forces between an actual
 355 state of the atmosphere and a reference state at rest (e.g., Holliday and McIntyre 1981;
 356 Andrews 1981). Following Novak and Tailleux (2018), the mean and eddy components of
 357 the local APE are defined as:

$$\text{mean APE} = \overline{\int_{\tilde{p}_r}^p \alpha([\theta], p'') - \alpha(\theta_r(p'', t), p'') dp''}, \quad (6)$$

$$\text{eddy APE} = \left[\overline{\int_{p_r}^{\tilde{p}_r} \alpha(\theta, p'') - \alpha(\theta_r(p'', t), p'') dp''} \right], \quad (7)$$

359 where α is the specific volume, θ is the potential temperature, θ_r the potential temperature
 360 of the reference state (which is, in this case, defined as the global area-weighted isobaric
 361 average of θ , equivalent to the reference state of Lorenz's APE), p is the pressure, and p_r
 362 and \tilde{p}_r are the reference pressures defined as:

$$\theta_r(p_r, t) = \theta \quad [\theta_r](\tilde{p}_r, t) = [\theta]. \quad (8)$$

363 The double prime denotes an integration variable. Again, the square brackets denote zonal
 364 mean and the bar is the time mean. More information on the local APE can be found in
 365 Tailleux (2013) and Novak and Tailleux (2018). The results below are integrated over the
 366 depth of the troposphere (i.e. 1000 - 200 hPa), and averaged over the mixing zone.

367 The responses of the mean APE are very sensitive to the choice of the mixing zone.
 368 However for some cases, such as most of the experiments in Fig. 6a and b (where the mixing
 369 zone was defined as the region where heat flux is within 55% of the maximum value), there
 370 is a correspondence with the responses of the baroclinicity, though the mean APE responses
 371 are somewhat weaker. For polar warming, the responses show less agreement but this can
 372 be corrected (at the expense of the other runs) by slightly changing the threshold value to
 373 redefine the mixing zone. The high sensitivity to the choice of the mixing zone also applies
 374 to the Lorenz APE definition.

375 This sensitivity is caused by the mean APE exhibiting a minimum at the latitudes of the
 376 storm tracks (Fig. 7, thin black contours), which is a consequence of both APE definitions

377 being defined to be proportional to the squared departures from a horizontally constant
378 reference state of potential temperature. This makes its responses largely non-local (Fig. 7,
379 colors), and if the responses are spatially complex as they are for the thermal forcing (Fig.
380 7c and d), then different signs of the responses can be obtained for slightly different heat
381 flux thresholds used to define the mixing zone (e.g. 30% and 70%, both of which have been
382 advocated by previous works). The mean APE is therefore not an ideal diagnostic for the
383 equilibration of storm tracks. This is in contrast with the maximum Eady growth rate or
384 the isentropic slope (below), both of which exhibit maxima in the center of storm tracks and
385 their responses are much less sensitive to the width of the mixing zone.

386 Eddy available potential and eddy kinetic energies (Fig. 6c - f) can be viewed as measures
387 of storm track activity, though one needs to be aware of the inclusion of barotropic waves
388 in these terms. The eddy APE changes in accordance with the eddy heat flux, showing a
389 consistent increase in the response to polar cooling and a weak sensitivity to eddy friction.
390 The eddy kinetic energy exhibits a more complex behavior, but its baroclinic component
391 (Fig. 6g and h), extracted as in Chen (1983), shows a very similar variability to that of the
392 eddy APE and eddy heat flux. Because both eddy energies exhibit maxima only within the
393 mixing zone, these responses are robust for both local and global averages.

394 The energy responses generally concur with the predicted two-way equilibration, but also
395 reveal additional spatial complexity in the mean APE. This is due to its non-local definition
396 and the confinement of the storm tracks to the mid-latitudes. This complexity is obscured
397 in the global Lorenz APE formulation, which may give a misleading picture of the APE
398 responses within storm tracks.

399 5. Criticality

400 As in Schneider and Walker (2006), criticality is defined as:

$$\xi = \frac{f}{\beta(p_0 - [p_t])} \frac{\overline{\partial_y[\theta]}}{\overline{\partial_p[\theta]}}, \quad (9)$$

401 where f is the Coriolis parameter, β its meridional derivative, p_0 the surface pressure and p_t
 402 the pressure of the tropopause (estimated using the WMO definition as the lowermost point
 403 where the lapse rate is equal to or lower than 2 K km^{-1}). $\overline{\partial_y[\theta]}/\overline{\partial_p[\theta]}$ is the isentropic slope
 404 computed as the ratio of the meridional and vertical potential temperature (zonal and time
 405 mean) gradients in the low-level atmosphere. This section evaluates criticality (and related
 406 quantities) on the 850 hPa level.

407 Before analyzing the bulk value of criticality, it is insightful to examine the f/β ratio
 408 and the spatial structure of the isentropic slope ($\overline{\partial_y[\theta]}/\overline{\partial_p[\theta]}$) separately, as shown in Fig. 8a
 409 and b for the reference runs only. The isentropic gradient was scaled to have dimensions
 410 of criticality, using the average f/β ratio across the baroclinic zone of the control run, and
 411 $(p_0 - \overline{p_t})^{-1} = R\overline{[T]}/gp\overline{[H]}$ with g being the gravitational acceleration, R the gas constant
 412 for ideal gas, T the temperature, p the pressure, and H the height of the tropopause of the
 413 restoration temperature profile.

414 As with baroclinicity and local mean APE, eddy friction increases the isentropic slope. In
 415 the case of the thermal forcing, the eddy-induced static stability response overcompensates
 416 again for the response in the meridional temperature gradient. This results in a decrease in
 417 the isentropic slope of the actual state despite the imposed increase of the isentropic slope
 418 in the temperature restoration field (T_r in Eq. 3). This overcompensation appears to be
 419 stronger than for baroclinicity, because the isentropic slope has a stronger dependence on
 420 N .

421 Fig. 8c and d show a summary of all responses in criticality, calculated using Eq. 9,
 422 again with a constant f/β ratio but with a varying tropopause height, and averaged over the
 423 baroclinic zone as in the previous section. The responses follow those of the isentropic slope,
 424 with a slight overcompensation by static stability causing some reduction with polar cooling.
 425 It is also evident that varying tropopause height has negligible effect on the criticality.

426 The signs of the responses change dramatically if criticality is calculated using f/β that
 427 is computed at the mean latitude of the storm track, defined by Levine and Schneider (2015)

428 as:

$$\phi_M = \frac{\int_{\phi_{\text{EQ}}}^{\phi_{\text{P}}} \overline{[v^* T^*]} \phi dy}{\int_{\phi_{\text{EQ}}}^{\phi_{\text{P}}} \overline{[v^* T^*]} dy}, \quad (10)$$

429 where ϕ is the latitude, and square brackets denote zonal mean and stars perturbations
430 thereof. ϕ_{EQ} and ϕ_{P} are the equatorward and poleward boundaries of the baroclinic zone,
431 respectively. Criticality appears to be more responsive to the thermal forcing than the eddy
432 friction (bottom panels of Fig. 8). The step-like structure of changes in Fig. 8 e and f is the
433 result of the low resolution of the model setting. The changes in the storm track latitude
434 (ranging between 38 and 44°) dominate the criticality response.

435 As opposed to the measures of eddy growth discussed above (i.e. baroclinicity, mean
436 APE and isentropic slope) the definition of criticality additionally includes β . If latitudinal
437 shifts of the storm track occur, then the β effect dominates and causes criticality to decrease
438 with a more equatorward position of the storm track. Green's (1960) study of analytical
439 models of baroclinic instability suggests that the β effect mainly reflects changes in the eddy
440 shape and size rather than changes in the eddy growth rate. This agrees with the apparent
441 difference between the responses of criticality and the other measures of eddy growth. The
442 other eddy growth measures are only weakly sensitive to the latitude of the storm track, and
443 they generally concur with the Ambaum-Novak predictions.

444 6. Discussion and conclusions

445 It has been shown that the seemingly counter-intuitive two-way equilibration of storm
446 tracks to extratropical thermal forcing and eddy friction, as predicted by the Ambaum-
447 Novak model, can be generally simulated in Earth-like model simulations. Eddies adjust to
448 changes in the thermal forcing of the mean baroclinicity, and the mean baroclinicity adjusts
449 to changes in the frictional dissipation of eddies.

450 The response to thermal forcing is equivalent to the generalized baroclinic adjustment
451 of the atmosphere (Zurita and Lindzen 2001; Zurita-Gotor 2007) and is reminiscent of the

452 eddy saturation phenomenon in the Southern Ocean (as studied by Munday et al. 2013).
453 Eddies act to maintain the flow near a point of baroclinic neutrality by limiting their own
454 growth rate. They do this both by reducing the meridional temperature gradient and by
455 increasing static stability via the horizontal and vertical heat fluxes respectively. Even in
456 quasi-geostrophic atmospheric models with constant static stability, the eddy meridional
457 heat flux is sufficient to keep the mean baroclinicity only weakly sensitive to the baroclin-
458 icity forcing (Zurita-Gotor and Vallis 2009). In the present GCM experiments the strong
459 responsiveness of eddies to increased thermal forcing is apparent in eddy heat flux, eddy
460 APE and baroclinic eddy kinetic energy.

461 In terms of the eddy friction-controlled equilibration, the maximum Eady growth rate,
462 mean APE and isentropic slope are all locally directly proportional to eddy dissipation while
463 the (baroclinic) eddy quantities are only weakly sensitive, as predicted. This relationship
464 has not been previously shown unambiguously, and it is argued here that it is the flip side
465 of the baroclinic adjustment phenomenon. These two relationships should be considered in
466 tandem in the context of the equilibration of storm tracks. Both of these relationships have
467 already been observed in simulations of the Southern Ocean, whereby oceanic eddies transfer
468 their energy via form drag to the bottom of the ocean where the energy dissipates (Marshall
469 et al. 2017).

470 However, the atmospheric GCM equilibration also includes characteristics that are not
471 predicted by the Ambaum-Novak model. The mid-latitude atmospheric response on a sphere
472 is spatially complex (more than in Marshall et al.’s (2017) channel model of the Southern
473 Ocean), due to the latitudinally restricted extent of the mid-latitude storm tracks. Beyond
474 the storm tracks the eddies are unable to modify the thermal structure of the atmosphere
475 substantially, and so care needs to be taken when interpreting variables (such as the mean
476 APE), whose definitions depend on the global atmospheric state.

477 It should also be noted that changing the Newtonian cooling term in the GCM experi-
478 ments (i.e., T_r in Eq. 3) is not exactly equivalent to changing the constant diabatic forcing

479 in the Ambaum-Novak model (i.e., F in Eq. 1). In addition, the Ambaum-Novak model
480 is also unable to predict the GCM's overcompensation by static stability in response to
481 thermal forcing, since the Ambaum-Novak model assumes a constant static stability. Quasi-
482 geostrophic scaling suggests that thermal forcing should affect the vertical heat fluxes more
483 strongly than the meridional heat fluxes (Zurita-Gotor and Vallis 2009). In other words, even
484 though the direct thermal forcing is to increase the mean meridional temperature gradient
485 (which is to a large extent reduced by horizontal eddy increased heat fluxes), the invigorated
486 eddies also increase the mean static stability (by their vertical heat fluxes). If the latter
487 effect dominates then the baroclinicity may be reduced (through the increased static stabil-
488 ity) even though the direct thermal forcing was to increase it (by increasing the meridional
489 temperature gradient). This overcompensation is apparent in the decreases in baroclinicity
490 in some of the GCM experiments in this study, and is more pronounced for the isentropic
491 slope (which has a higher dependency on static stability than the maximum Eady growth
492 rate or the mean APE). The strength of this overcompensation also decreases with increasing
493 eddy friction.

494 There are also limitations of using the GCM to simulate the atmospheric storm tracks.
495 Firstly, Held-Suarez GCMs have additional nonlocal eddy dissipation through thermal re-
496 laxation due to the Newtonian cooling approximation. Moreover, Zhang and Stone (2011)
497 have found that, for a coupled atmosphere-ocean system, boundary layer processes are de-
498 termined by thermal damping and the baroclinic adjustment can only be achieved in the
499 free troposphere. The GCM in this study cannot reproduce these boundary layer processes
500 that are more characteristic of the real atmosphere. Furthermore, moisture effects were ne-
501 glected, and the associated latent heat release and cloud feedbacks are likely to alter the
502 precise sensitivity of the equilibration (e.g., Hoskins and Valdes 1990; Voigt and Shaw 2015;
503 Ceppi et al. 2017). It would therefore be insightful to repeat the above analysis in a more
504 realistic coupled model.

505 As well as the limitations of the GCM, the fact that the Ambaum-Novak model lacks

506 nonlinear barotropic interactions between eddies and the mean flow (e.g. wave breaking) and
507 parametrizes all (direct and indirect) eddy effects into a single variable may be attributed to
508 the smaller sensitivity of GCM responses relative to the predicted responses. Nevertheless,
509 since other studies that used simpler channel models (e.g., Zhang et al. 2012; Marshall et al.
510 2017) were able to recover a much stronger dependence than the present results, it is more
511 likely that this relatively small sensitivity is specific to using a GCM, rather than being due
512 to an inability of the Ambaum-Novak model to predict the fundamental equilibration.

513 It should be noted that the theoretical prediction of this two-way equilibration is not
514 a unique feature of the Ambaum-Novak model. In fact, parallels can be drawn with both
515 Lorenz’s (1984) and Thompson’s (1987) models, as discussed in Novak et al. (2017). In
516 essence, both types of equilibration ensure that in a steady state eddy dissipation rate
517 matches the eddy growth rate (baroclinicity), and that the forcing of the baroclinicity
518 matches the baroclinicity erosion by eddies. The presence of this two-way equilibration
519 in theoretical models, as well as in atmospheric and oceanic GCMs, suggests that this is a
520 general feature of baroclinically unstable systems.

521 In terms of the potential implications on the large scale circulation, shifts in the over-
522 turning circulation and the associated mid-latitude jet (as well as the eddy momentum fluxes
523 - not shown) were found to be of a comparable magnitude for the thermal forcing and eddy
524 friction, despite the non-symmetric responses in baroclinicity and baroclinic eddies. Al-
525 though a detailed consideration of momentum exchanges in this two-way equilibration is
526 the subject of a different study, the existence of the two-way equilibration indicates that
527 the baroclinicity-eddy exchanges are the primary responses, concurring with the numerical
528 solutions described in Hart (1979). Nevertheless, the responses of the momentum fluxes
529 and the meridional overturning circulation are still an important factor that determines the
530 three-dimensional properties of the baroclinic zone (e.g., Zurita-Gotor and Lindzen 2004;
531 Blanco-Fuentes and Zurita-Gotor 2011; Nie et al. 2013).

532 The comparable shifts in the latitude of the eddy-driven circulation further demonstrate

533 that such shifts are not linearly related to the storm track activity (a causal link often used
534 to explain jet shifts in climate models). This agrees with existing theories (e.g., Thorncroft
535 et al. 1993; Orlanski 2003; Rivière 2009), which suggest that latitudinal jet shifts can be
536 induced by changes in either baroclinicity (which can modulates the sign of the dominant
537 momentum fluxes) or the strength of baroclinic eddies (due to their default preference to
538 supply poleward momentum fluxes into the jet). The lack of symmetry of the two-way
539 equilibration of baroclinicity and baroclinic eddies (and their independent ability to modify
540 the mean flow) may help better to understand the uncertainty in the responses of the mid-
541 latitude storm tracks and the associated jets predicted by comprehensive climate models
542 (Shepherd 2014). We are currently analyzing the combined biases in baroclinicity and heat
543 fluxes in such climate models.

544 The rest of this section addresses the seemingly contradictory issues with previous lit-
545 erature outlined in the introduction. Firstly, both the global mean APE and eddy kinetic
546 energy have been observed to increase with radiative forcing of storm tracks (O’Gorman and
547 Schneider 2008, O’Gorman 2010), yet the Ambaum-Novak model predicts that the mean
548 APE should be insensitive to this forcing (and storm track activity). The mean APE re-
549 sponses have been found to be spatially complex, and very sensitive to the choices used to
550 define the baroclinic mixing zone, over which the mean APE is averaged. For wide enough
551 mixing zones, a directly proportional relationship between the forcing and mean APE can
552 be found (though this relationship weakens for stronger eddy friction), which is broadly
553 consistent with the previous studies. It is argued here that due to the nonlocal nature of
554 its definition, APE is not a good diagnostic of storm track equilibration. Nevertheless, it
555 still agrees locally with the characteristics of the baroclinic adjustment and the dissipative
556 control discussed above.

557 Secondly, Chen et al. (2007) have found a strong dependency of eddy kinetic energy to
558 global eddy frictional dissipation. In the experiments presented here this is true for the
559 barotropic part of the eddy kinetic energy, but not for the baroclinic component. The latter

560 is proportional to eddy APE, both of which are only weakly and non-monotonically sensitive
561 to eddy friction (generally agreeing with the Ambaum-Novak predictions). Similarly, in the
562 experiments of O’Gorman and Schneider (2008) mentioned above, the eddy kinetic energy
563 is not divided into its barotropic and baroclinic parts, which may be responsible for the
564 observed proportionality between the mean APE and eddy kinetic energy when responding
565 to changes in radiative forcing. More insight may be gained by isolating the high-frequency
566 transient eddies from planetary-scale Rossby waves, which have been found to have opposite
567 effects on the mean flow (Hoskins et al. 1983).

568 To conclude, the two-way equilibration to thermal forcing and eddy friction predicted
569 by purely baroclinic theory can be observed in primitive equations of atmospheric, as well
570 as oceanic, GCMs. This equilibration is characterized by a strong response in eddy growth
571 rate (measured by baroclinicity-like quantities) to eddy friction and a strong response in
572 baroclinic eddy intensity to a mean temperature gradient forcing. The two-way equilibration
573 is of relevance to climate modeling studies, where the circulation response to changes in the
574 global radiation and eddy dissipative parameterizations is still not fully understood.

575 *Acknowledgments.*

576 This work is supported by the U.K. Natural Environment Research Council [grant number
577 NE/M014932/1], and we thank our reviewers for their very helpful feedback.

REFERENCES

- 580 Ambaum, M. H. P. and L. Novak, 2014: A nonlinear oscillator describing storm track vari-
581 ability. *Quart. J. Roy. Meteor. Soc.*, **140**, 2680–2684.
- 582 Andrews, D. G., 1981: A note on potential energy density in a stratified compressible fluid.
583 *J. Fluid Mech.*, **107**, 227–236.
- 584 Blanco-Fuentes, J. and P. Zurita-Gotor, 2011: The driving of baroclinic anomalies at different
585 timescales. *Geophys. Res. Lett.*, **38 (23)**, 123805.
- 586 Ceppi, P., F. Brient, M. D. Zelinka, and D. L. Hartmann, 2017: Cloud feedback mechanisms
587 and their representation in global climate models. *WIREs Climate Change*, doi:10.1002/
588 wcc.465.
- 589 Chen, G., I. M. Held, and W. A. Robinson, 2007: Sensitivity of the latitude of the surface
590 westerlies to surface friction. *J. Atmos. Sci.*, **64**, 2899–2915.
- 591 Chen, T.-C., 1983: The energy exchange between the baroclinic and barotropic components
592 of atmospheric flow in the tropics during the FGGE summer. *Monthly Weather Review*,
593 **111 (7)**, 1389–1396.
- 594 Fraedrich, K., E. Kirk, U. Luksch, and F. Lunkeit, 2005: The Portable University Model of
595 the Atmosphere (PUMA): Storm track dynamics and low frequency variability. *Meteorol.*
596 *Zeitschrift*, **14**, 735–745.
- 597 Fraedrich, K., E. Kirk, and F. Lunkeit, 1998: PUMA: Portable University Model of the
598 Atmosphere. Technical Report 16, Deutsches Klimarechenzentrum, 38 pp.
- 599 Green, J. S. A., 1960: A problem in baroclinic stability. *Quart. J. Roy. Meteor. Soc.*, **86**,
600 237–251.

- 601 Hart, J. E., 1979: Finite amplitude baroclinic instability. *Annu. Rev. Fluid Mech.*, **11** (1),
602 147–172.
- 603 Harvey, B., L. Shaffrey, and T. Woollings, 2013: Equator-to-pole temperature differences
604 and the extra-tropical storm track responses of the CMIP5 climate models. *Clim. Dyn.*,
605 **33**, 1171–1182.
- 606 Held, I. M. and M. J. Suarez, 1994: A proposal for the intercomparison of the dynamical
607 cores of atmospheric general circulation model. *Bull. Amer. Meteor. Soc.*, **75**, 1825–1830.
- 608 Holliday, D. and M. E. McIntyre, 1981: On potential energy density in an incompressible
609 stratified fluid. *J. Fluid Mech.*, **107**, 221–225.
- 610 Hoskins, B., I. James, and G. White, 1983: The shape, propagation and mean-flow interac-
611 tion of large-scale weather systems. *J. Atmos. Sci.*, **40**, 1595–1612.
- 612 Hoskins, B. J. and K. I. Hodges, 2005: A new perspective on Southern Hemisphere storm
613 tracks. *J. Climate*, **18**, 4108–4129.
- 614 Hoskins, B. J. and A. J. Simmons, 1975: A multi-layer spectral model and the semi-implicit
615 method. *Quart. J. Roy. Meteor. Soc.*, **101**, 637–655.
- 616 Hoskins, B. J. and P. J. Valdes, 1990: On the existence of storm-tracks. *J. Atmos. Sci.*, **47**,
617 1854–1864.
- 618 James, I. N., 1994: *Introduction to Circulating Atmospheres*. Cambridge University Press,
619 Cambridge, pp. 230.
- 620 Jansen, M. and R. Ferrari, 2012: Macroturbulent equilibration in a thermally forced primitive
621 equation system. *J. Atmos. Sci.*, **69**, 695–713.
- 622 Jansen, M. and R. Ferrari, 2013: Equilibration of an atmosphere by adiabatic eddy fluxes.
623 *J. Atmos. Sci.*, **70**, 2948–2962.

- 624 Kim, H. K. and S. Lee, 2001: Hadley cell dynamics in a primitive equation model. part II:
625 Nonaxisymmetric flow. *J. Atmos. Sci.*, **58**, 2859–2871.
- 626 Kållberg, P., P. Berrisford, B. Hoskins, A. Simmons, S. Uppala, S. Lamy-Thépaut, and
627 R. Hine, 2005: *ERA-40 Atlas*. 19, ECMWF.
- 628 Levine, X. J. and T. Schneider, 2015: Baroclinic eddies and the extent of the hadley circu-
629 lation: An idealized GCM study. *J. Atmos. Sci.*, **72** (7), 2744–2761.
- 630 Lorenz, E. N., 1955: Available potential energy and the maintenance of the general circula-
631 tion. *Tellus*, **7**, 157–167.
- 632 Lorenz, E. N., 1984: Irregularity: a fundamental property of the atmosphere. *Tellus*, **36A**,
633 98–110.
- 634 Marshall, D. P., M. H. P. Ambaum, J. R. Maddison, D. Munday, and L. Novak, 2017: Eddy
635 saturation and frictional control of the Antarctic Circumpolar Current. *Geophys. Res.*
636 *Lett.*, **44**, 286–292.
- 637 Mbengue, C. and T. Schneider, 2013: Storm track shifts under climate change: What can
638 be learned from large-scale dry dynamics. *J. Climate*, **26**, 9923–9930.
- 639 Mbengue, C. O. and T. Schneider, 2018: Linking Hadley circulation and storm tracks
640 in a conceptual model of the atmospheric energy balance. *J. Atmos. Sci.*, **in press**,
641 <https://doi.org/10.1175/JAS-D-17-0098.1>.
- 642 Munday, D. R., H. L. Johnson, and D. P. Marshall, 2013: Eddy saturation of equilibrated
643 circumpolar currents. *J. Phys. Oceanogr.*, **43**, 507–532.
- 644 Nie, Y., Y. Zhang, X.-Q. Yang, and G. Chen, 2013: Baroclinic anomalies associated with
645 the southern hemisphere annular mode: Roles of synoptic and low-frequency eddies. *Geo-*
646 *physical Research Letters*, **40** (10), 2361–2366.

- 647 Novak, L., M. H. P. Ambaum, and R. Tailleux, 2015: The lifecycle of the North Atlantic
648 storm track. *J. Atmos. Sci.*, **72**, 821–833.
- 649 Novak, L., M. H. P. Ambaum, and R. Tailleux, 2017: Marginal stability and predator-prey
650 behaviour within storm tracks. *Quart. J. Roy. Meteor. Soc.*, **143**, 1421–1433.
- 651 Novak, L. and R. Tailleux, 2018: On the local view of atmospheric available potential energy.
652 *J. Atmos. Sci.*, **in press**, doi:10.1175/JAS-D-17-0330.1.
- 653 O’Gorman, P. A., 2010: Understanding the varied response of the extratropical storm tracks
654 to climate change. *Proc. Natl. Acad. Sci. (USA)*, **107**, 19176–19180.
- 655 O’Gorman, P. A. and T. Schneider, 2007: Recovery of atmospheric flow statistics in a
656 general circulation model without nonlinear eddy-eddy interactions. *Geophys. Res. Lett.*,
657 **37**, l22801.
- 658 O’Gorman, P. A. and T. Schneider, 2008: Energy of midlatitude transient eddies in idealized
659 simulations of changed climates. *J. Clim.*, **21**, 5797–5806.
- 660 Oort, A. H., 1964: On estimates of the atmospheric energy cycle. *Mon. Weather Rev.*,
661 **92 (11)**, 483–493.
- 662 Orlandi, I., 2003: Bifurcation in eddy life cycles: Implications for storm track variability.
663 *J. Atmos. Sci.*, **60**, 993–1023.
- 664 Pedlosky, J., 1992: *Geophysical Fluid Dynamics*. Springer, New York, 230 pp.
- 665 Pithan, F., T. G. Shepherd, Z. G., and I. Sandu, 2016: Climate model biases in jet streams,
666 blocking and storm tracks resulting from missing orographic drag. *Geophys. Res. Lett.*,
667 **43**, 7231–7240.
- 668 Polichtchouk, I. and T. G. Shepherd, 2016: Zonal-mean circulation response to reduced
669 air–sea momentum roughness. *Q. J. R. Meteor. Soc.*, **142**, 2611–2622.

670 Rivière, G., 2009: Effect of latitudinal variations in low-level baroclinicity on eddy life cycles
671 and upper-tropospheric wave-breaking processes. *J. Atmos. Sci.*, **66**, 1569–1592.

672 Schneider, E. K., 1981: On the amplitudes reached by baroclinically unstable disturbances.
673 *J. Atmos. Sci.*, **38**, 2142–2149.

674 Schneider, T. and C. C. Walker, 2006: Self-organization of atmospheric macroturbulence into
675 critical states of weak nonlinear eddy- eddy interactions. *J. Atmos. Sci.*, **63**, 1569–1586.

676 Schneider, T. and C. C. Walker, 2008: Scaling laws and regime transitions of macroturbu-
677 lence in dry atmospheres. *J. Atmos. Sci.*, **65**, 2153–2173.

678 Shepherd, T. G., 2014: Atmospheric circulation as a source of uncertainty in climate change
679 projections. *Nature Geoscience*, **7**, 703–708.

680 Stone, P. H., 1978: Baroclinic adjustment. *J. Atmos. Sci.*, **35**, 561–571.

681 Tailleux, R., 2013: Available potential energy density for a multicomponent Boussinesq fluid
682 with arbitrary nonlinear equation of state. *J. Fluid Mech.*, **735**, 499–518.

683 Thompson, P. D., 1987: Large-scale dynamical response to differential heating: Statistical
684 equilibriumstates and amplitude vacillation. *J. Atmos. Sci.*, **44**, 1237–1248.

685 Thorncroft, C. D., B. J. Hoskins, and M. E. McIntyre, 1993: Two paradigms of baroclinic
686 wave life-cycle behaviour. *Quart. J. Roy. Meteor. Soc.*, **119**, 17–55.

687 Voigt, A. and T. A. Shaw, 2015: Circulation response to warming shaped by radiative
688 changes of clouds and water vapour. *Nature Geosci.*, **8**, 102–106.

689 Zappa, G., M. K. Hawcroft, L. Shaffrey, E. Black, and D. J. Brayshaw, 2015: Extratropical
690 cyclones and the projected decline of winter mediterranean precipitation in the cmip5
691 models. *Climate Dynamics*, **45** (7), 1727–1738.

- 692 Zappa, G., G. Masato, L. Shaffrey, T. Woollings, and K. Hodges, 2014: Linking northern
693 hemisphere blocking and storm track biases in the cmip5 climate models. *Geophys. Res.*
694 *Lett.*, **41** (1), 135–139.
- 695 Zhang, Y. and P. H. Stone, 2011: Baroclinic adjustment in an atmosphere–ocean thermally
696 coupled model: The role of the boundary layer processes. *J. Atmos. Sci.*, **68**, 2710–2730.
- 697 Zhang, Y., X.-Q. Yang, Y. Nie, and G. Chen, 2012: Annular mode–like variation in a
698 multilayer quasigeostrophic model. *J. Atmos. Sci.*, **69**, 2940–2958.
- 699 Zurita, P. and R. S. Lindzen, 2001: The equilibration of short Charney waves: Implications
700 for potential vorticity homogenization in the extratropical troposphere. *J. Atmos. Sci.*,
701 **58**, 3443–3462.
- 702 Zurita-Gotor, P., 2007: The relation between baroclinic adjustment and turbulent diffusion
703 in the two-layer model. *J. Atmos. Sci.*, **64**, 1284–1300.
- 704 Zurita-Gotor, P. and R. S. Lindzen, 2004: Baroclinic equilibration and the maintenance of
705 the momentum balance. part ii: 3D results. *J. Atmos. Sci.*, **61**, 1483–1499.
- 706 Zurita-Gotor, P. and G. K. Vallis, 2009: Equilibration of baroclinic turbulence in primitive
707 equations and quasigeostrophic models. *J. Atmos. Sci.*, **66** (4), 837–863.

708 List of Figures

- 709 1 Meridional structure of the weight applied to the eddy friction timescale (w_f)
710 and the weight applied to the barotropic temperature anomaly (w_T) used
711 in the forced experiments. The precise formulation of these weights is not
712 essential, but for the sake of completion $w_f = \max[0, -(0.05\phi^{-8} + 0.01\phi^2 -$
713 $1)(1 - \cos^2 2\phi)]$ and $w_T = \max[0, -(0.1\phi^8 + 1)^{-1} + 1]$. Note that both weights
714 were normalized so that the highest value is one. 32
- 715 2 Control experiment, showing (left) the zonal mean zonal wind (contours,
716 showing 10,20 and 30 m s⁻¹) and the mean meridional overturning circu-
717 lation (colors, in kg s⁻¹), and (right) the potential temperature (colors, in K),
718 meridional heat flux (thin contours, showing 5, 10, 15 and 20 K m s⁻¹) and
719 maximum Eady growth rate (thick black contour, 0.5 day⁻¹). 33
- 720 3 Mass weighted average of the overturning streamfunction between 925 and 250
721 hPa (colors, in kg s⁻¹), and thermal wind (black contours, in m s⁻²; defined as
722 the difference between upper level (250-200 hPa) and low-level (925-700 hPa)
723 zonal wind) for the reference runs when either eddy friction (a) or thermal
724 forcing (b) are changed. Dashed contours mark negative values. The tick
725 marks are placed at values tested by the numerical experiments. 34
- 726 4 Low-level heat flux (a,b), maximum Eady growth rate (c,d), meridional po-
727 tential temperature gradient (e,f) and squared static stability (g,h), for the
728 reference runs, i.e. experiments where either eddy friction (left) or thermal
729 forcing (right) were changed. 35
- 730 5 Baroclinicity (a, b; at 775 hPa) and heat flux (c, d; at 850 hPa) for all
731 experiments, both averaged in latitude over the mixing zone (see text for
732 details). Each line in the panels on the left marks experiments with the same
733 thermal forcing, and each line on the right marks experiments with the same
734 eddy friction. 36

- 735 6 Same as Fig. 5, but for the local mean APE (a, b; integrated vertically
736 and averaged over the baroclinic zone), global eddy APE (c, d), global eddy
737 kinetic energy (e, f), and global baroclinic eddy kinetic energy (g, h). The
738 global energy terms were computed as in Lorenz (1955), and the eddy kinetic
739 energy was split into its baroclinic part as per Chen (1983). Units are 10^5 J
740 m^{-2} . 37
- 741 7 Time-mean local mean APE (calculated using Eq. 6) responses. The thin
742 black contours show the absolute values of the control run (starting at 5×10^5
743 J kg^{-1} in the mid-latitudes with intervals of $5 \times 10^5 \text{ J kg}^{-1}$). In color shading
744 are the anomalies from the control run of the extreme cases of the reference
745 runs, namely showing the runs of lowest (a) and highest (b) eddy friction,
746 and the highest (c) and lowest (d) polar cooling. Units are 10^4 J kg^{-1} . The
747 absolute values of the heat flux field are also shown in the thick black contours
748 (starting at 5 with intervals of 5 K m s^{-1}). 38
- 749 8 Low-level dimensionless criticality response displayed as (a, b) a scaled isen-
750 tropic slope (colors) for the reference runs, (c, d) the isentropic slope scaled
751 with a variable tropopause height and constant f/β for all runs, and (e, f)
752 criticality using a variable tropopause height and variable f/β for all runs. (c,
753 d, e, f) are averaged over the baroclinic zone and computed on the 850 hPa
754 level. (a, b) also display the values of the f/β ratio (in 10^5 m). 39

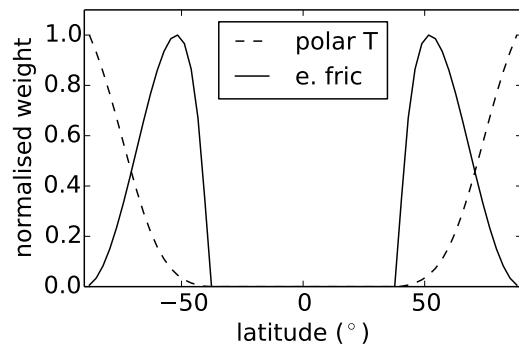


FIG. 1. Meridional structure of the weight applied to the eddy friction timescale (w_f) and the weight applied to the barotropic temperature anomaly (w_T) used in the forced experiments. The precise formulation of these weights is not essential, but for the sake of completion $w_f = \max[0, -(0.05\phi^{-8} + 0.01\phi^2 - 1)(1 - \cos^2 2\phi)]$ and $w_T = \max[0, -(0.1\phi^8 + 1)^{-1} + 1]$. Note that both weights were normalized so that the highest value is one.

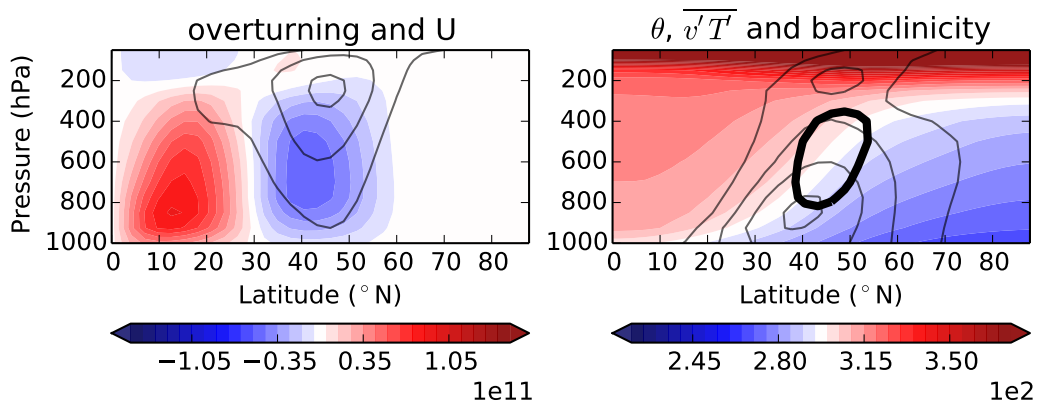


FIG. 2. Control experiment, showing (left) the zonal mean zonal wind (contours, showing 10,20 and 30 m s^{-1}) and the mean meridional overturning circulation (colors, in kg s^{-1}), and (right) the potential temperature (colors, in K), meridional heat flux (thin contours, showing 5, 10, 15 and 20 K m s^{-1}) and maximum Eady growth rate (thick black contour, 0.5 day^{-1}).

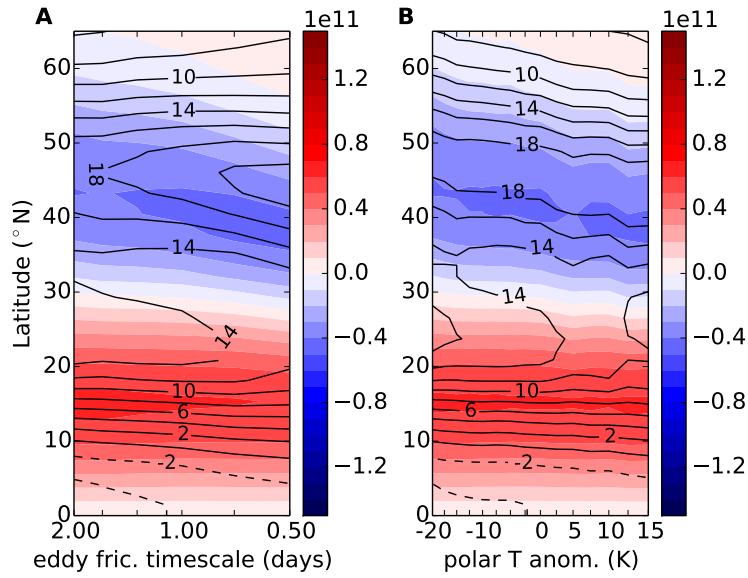


FIG. 3. Mass weighted average of the overturning streamfunction between 925 and 250 hPa (colors, in kg s^{-1}), and thermal wind (black contours, in m s^{-2} ; defined as the difference between upper level (250-200 hPa) and low-level (925-700 hPa) zonal wind) for the reference runs when either eddy friction (a) or thermal forcing (b) are changed. Dashed contours mark negative values. The tick marks are placed at values tested by the numerical experiments.

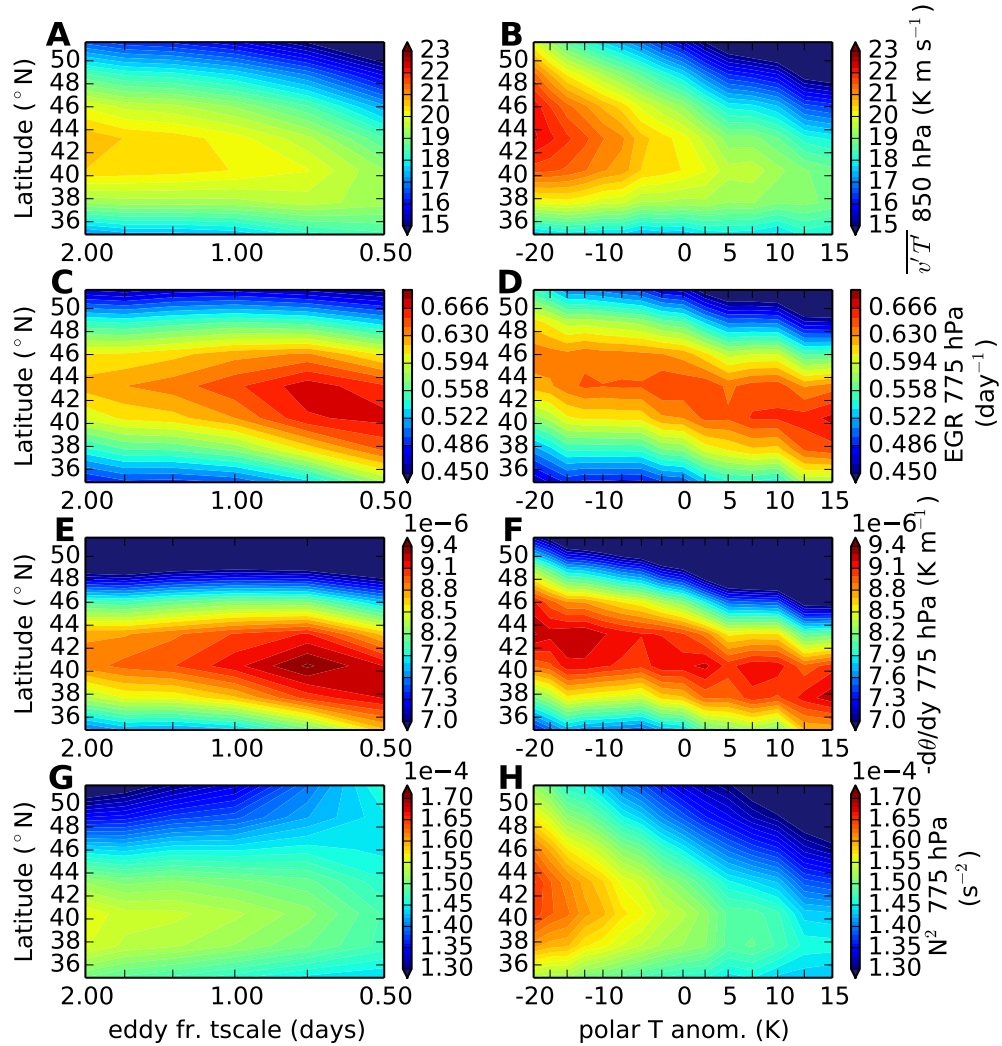


FIG. 4. Low-level heat flux (a,b), maximum Eady growth rate (c,d), meridional potential temperature gradient (e,f) and squared static stability (g,h), for the reference runs, i.e. experiments where either eddy friction (left) or thermal forcing (right) were changed.

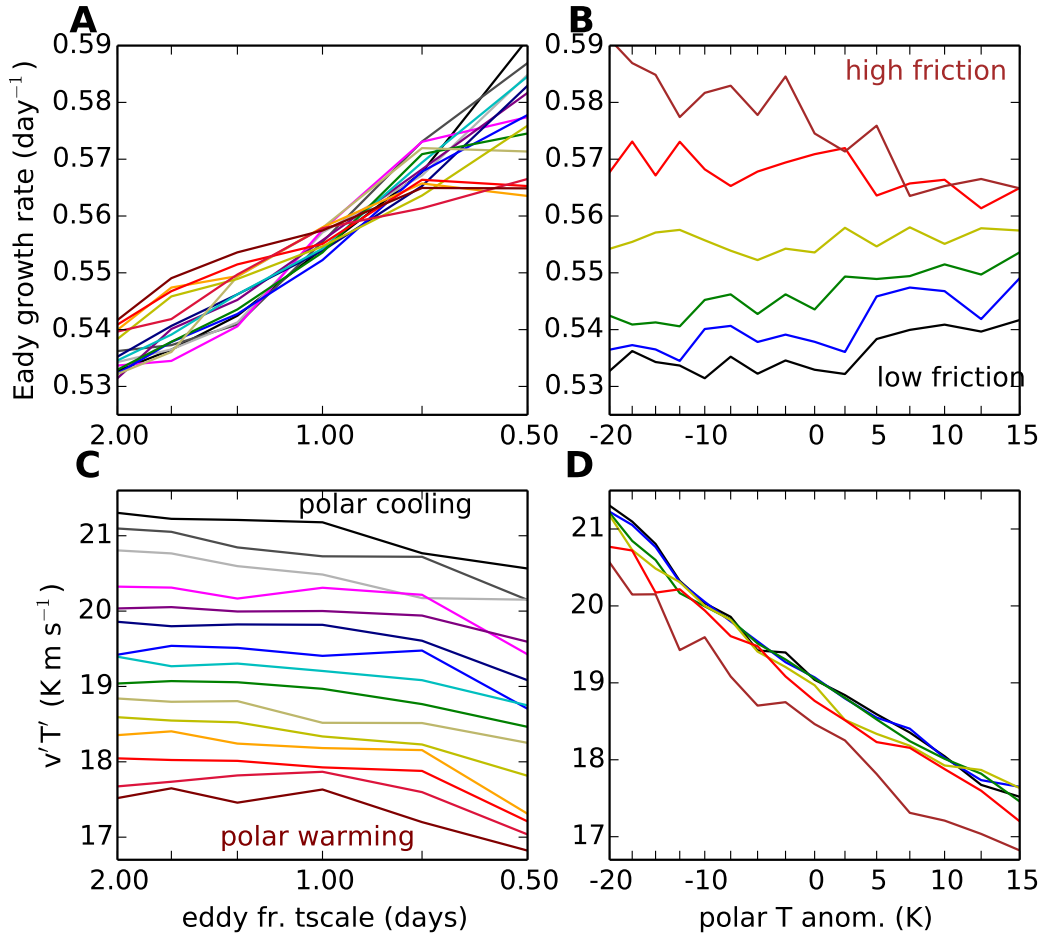


FIG. 5. Baroclinicity (a, b; at 775 hPa) and heat flux (c, d; at 850 hPa) for all experiments, both averaged in latitude over the mixing zone (see text for details). Each line in the panels on the left marks experiments with the same thermal forcing, and each line on the right marks experiments with the same eddy friction.

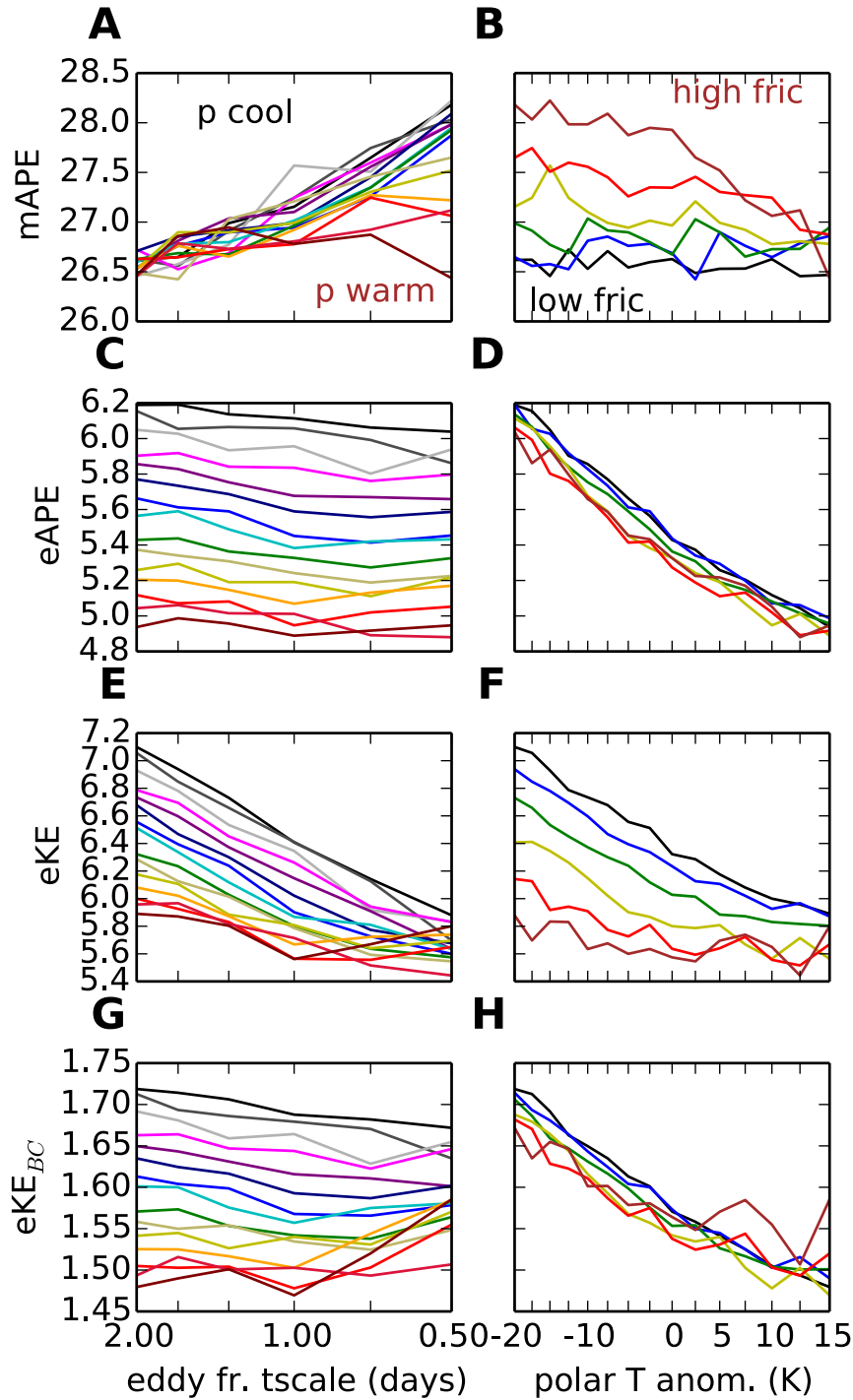


FIG. 6. Same as Fig. 5, but for the local mean APE (a, b; integrated vertically and averaged over the baroclinic zone), global eddy APE (c, d), global eddy kinetic energy (e, f), and global baroclinic eddy kinetic energy (g, h). The global energy terms were computed as in Lorenz (1955), and the eddy kinetic energy was split into its baroclinic part as per Chen (1983). Units are 10^5 J m^{-2} .

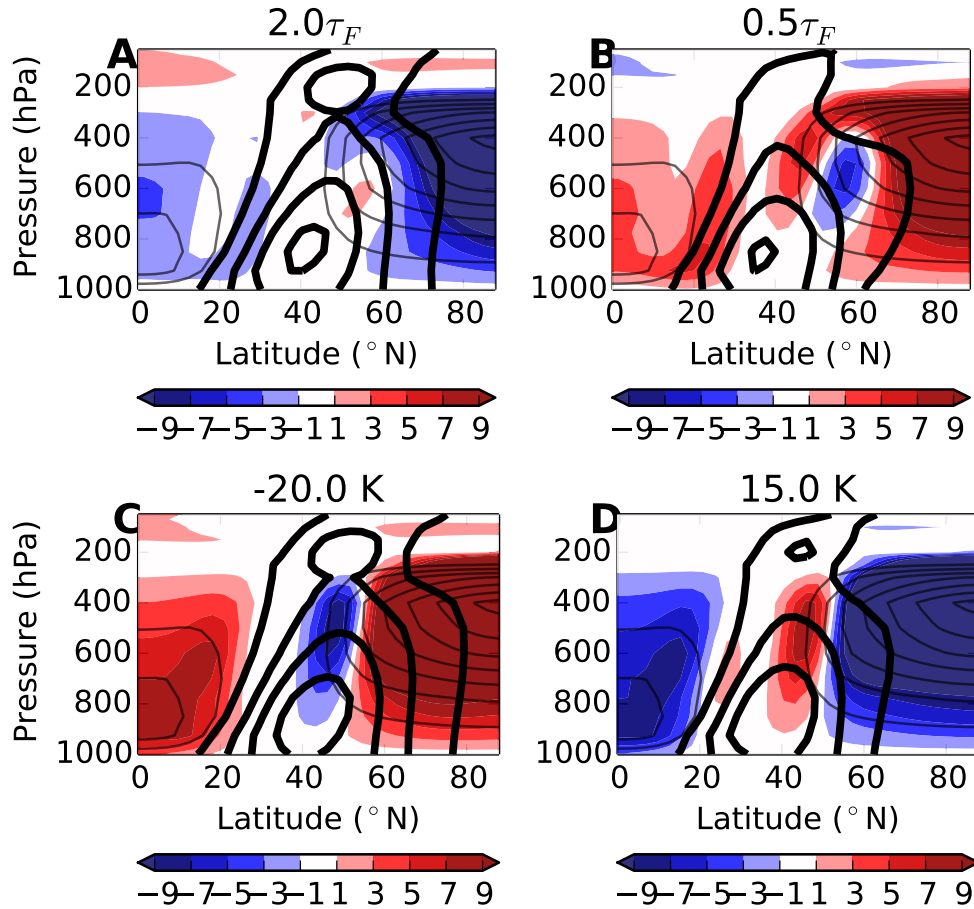


FIG. 7. Time-mean local mean APE (calculated using Eq. 6) responses. The thin black contours show the absolute values of the control run (starting at $5 \times 10^5 \text{ J kg}^{-1}$ in the mid-latitudes with intervals of $5 \times 10^5 \text{ J kg}^{-1}$). In color shading are the anomalies from the control run of the extreme cases of the reference runs, namely showing the runs of lowest (a) and highest (b) eddy friction, and the highest (c) and lowest (d) polar cooling. Units are 10^4 J kg^{-1} . The absolute values of the heat flux field are also shown in the thick black contours (starting at 5 with intervals of 5 K m s^{-1}).

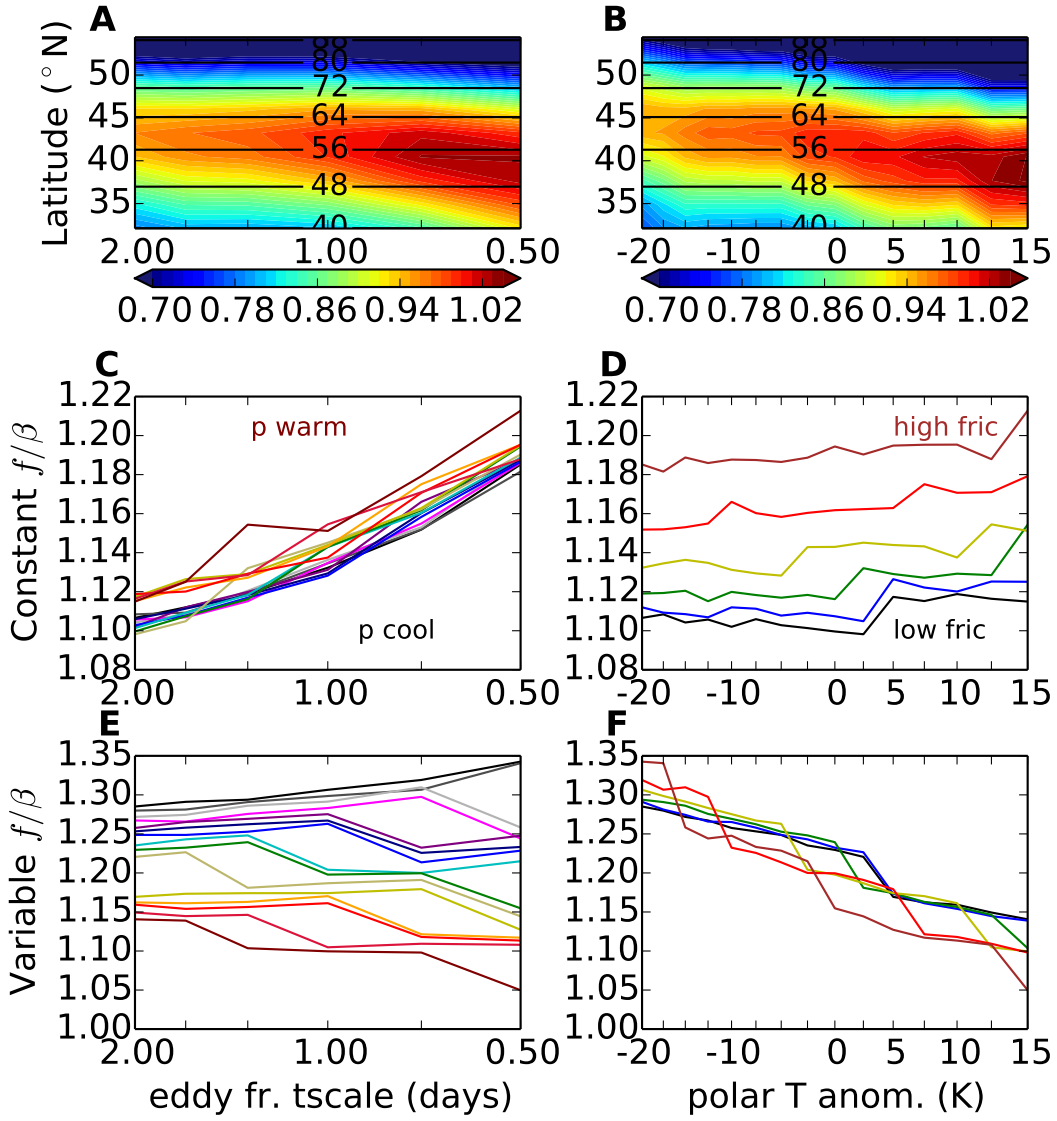


FIG. 8. Low-level dimensionless criticality response displayed as (a, b) a scaled isentropic slope (colors) for the reference runs, (c, d) the isentropic slope scaled with a variable tropopause height and constant f/β for all runs, and (e, f) criticality using a variable tropopause height and variable f/β for all runs. (c, d, e, f) are averaged over the baroclinic zone and computed on the 850 hPa level. (a, b) also display the values of the f/β ratio (in 10^5 m).